Flow stratification in the horizontal pipe with heated supercritical CO_2

X. Chu, E. Laurien and D. M. McEligot*

University of Stuttgart / Institute of Nuclear Technology and Energy Systems
Pfaffenwaldring 31, D-70569 Stuttgart, Germany, +49 711 685 62415, Laurien@ike.uni-stuttgart.de
* Nuclear Engineering Division, Univ. Idaho, 995 University Blvd., Idaho Falls, Idaho 83401 USA

Topic: sCO₂ Fluid Mechanics & Heat Transfer

Abstract:

In the current research, heat transfer of supercritical CO_2 in a horizontal pipe is investigated using direct numerical simulation (DNS) for the first time. Well resolved DNS eliminates the uncertainty brought by turbulence modelling. The small pipe diameter (D=1,2 mm) and moderately low inlet Reynolds number Re_0=5400 is similar as the channel flow in the compact heat exchanger (PCHE). Inflow temperature (T_0=301.15 K) is set to be lower than pseudo-critical temperature T_{pc}. Thermo-physical properties change rapidly when fluid temperature rises across T_{pc} under heating condition. In the present DNS, wall temperature T_w is found to be strongly inhomogeneous in the circumferential direction. T_w is gratefully higher on the top surface than on the bottom surface. As a result of buoyancy, flow stratification is developed by the secondary flow, which means the heated light fluid flows to the top region. The streamwise velocity field $\tilde{U}_z$ is also modified by the flow stratification. Low-speed fluid near the circumferential wall is heated firstly and transported to the top region by the secondary flow. High-speed bulk fluid is concentrated at the bottom as a result of high density. The modification of velocity field affects the shear production for turbulence near the top surface. Turbulent kinetic energy (TKE) is strongly suppressed in this region, which is also the same for the field of radial turbulent heat flux. The convective heat transfer in this direction is attenuated and it enhances the flow stratification.

1. Introduction

Using supercritical fluid in a power cycle is widely considered as an advanced solution. High efficiency, compact size, and reduced complexity are the main advantage of these cycles [1]. Most recent fossil power plant uses supercritical water Rankine cycle to increase the thermal efficiency to about 45% [2]. Supercritical Water-Cooled Reactor (SCWR) is chosen as one of Generation IV nuclear reactor concept, which is also called as HPLWR in Europa. Besides, supercritical CO_2 power cycle is being intensively researched for high temperature solar, nuclear and fossil energy. Supercritical fluids have distinctive properties. At supercritical pressure, the fluid phase change from liquid to gas does not exist as in subcritical flows. When temperature rises across the pseudo-critical point (T_{pc}), the density (ρ), the thermal conductivity (κ) and the dynamic viscosity (μ) decrease drastically, the specific heat capacity (C_p) shows a peak in a very narrow temperature range. Fig.1 shows the variable properties of CO_2 as a function of the temperature (T) at a constant pressure P=8 MPa, which is above the critical pressure.
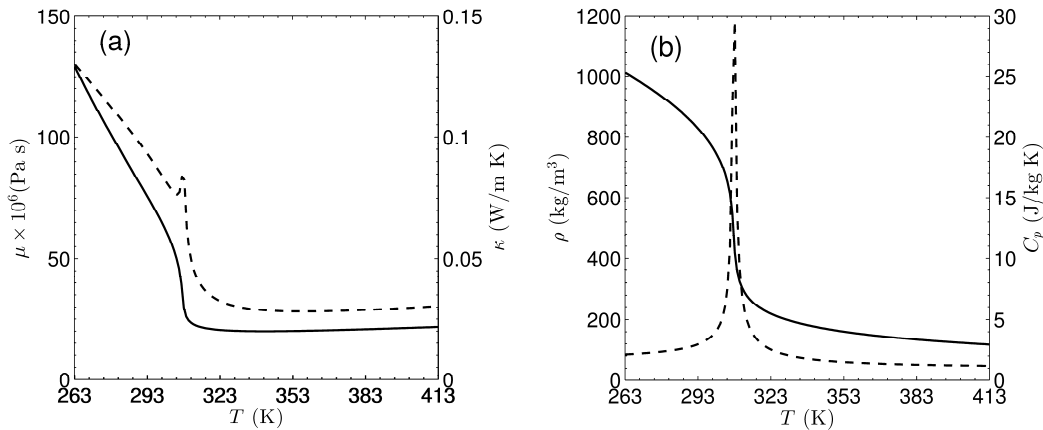
Figure 2: Variation of thermo-physical properties viscosity μ ((a), '-'), heat conductivity κ ((a), '--'), density ρ ((b), '-') and heat capacity C_p ((b), '--') of CO_2 as a function of the temperature at a supercritical pressure of P_0 = 8 MPa, data from NIST data base

Significant property variations lead to complex heat transfer phenomenon. Heat transfer enhancement and deterioration have been observed in the vertical flowing pipe. A recent review of these early works is written by Jackson [3], and a more comprehensive one by Duffey and Pioro [2]. Most of the experiments can only deliver measurement of wall temperature on the pipe surface without any detailed flow statistics in the pipe. Numerical approach based on the Reynolds-averaged Navier-Stokes Equations (RANS) has been also tried to investigate these phenomena [4]. Experience shows that classical- even advanced turbulence modelling is not reliable to reproduce the heat transfer deterioration and recovery. Direct numerical simulation (DNS) is until now still rare in this area. Bae et al. [5] uses an in-house DNS code for vertical pipe flow at Re_0=5400. Recently, Nemati et al. [6] accomplished another DNS study and mentioned some discrepancy with Bae et al. under the same simulation conditions.

Compared with the research to the vertical pipe, horizontal pipe flow draws less attention. The horizontal pipe with heated supercritical CO_2 has also broad industrial applications, such as printed circuit heat exchanger (PCHE). PCHE is attractive as a high efficient heat exchanger with compact size. In PCHE, supercritical CO_2 flows through the cold channel horizontally and is heated by the hot channel. Adebiy and Hall [7] conducted an experimental investigation of heat transfer to supercritical pressure CO_2 in a horizontal pipe. It was observed that heat transfer at the bottom of the pipe is enhanced and at the top is reduced by buoyancy. Bazargan [8] introduced the effect of buoyancy on heat transfer in supercritical water flow in a horizontal tube experimentally. Liao et al. in his work [9] focused on measuring the heat transfer coefficients from supercritical CO_2 flowing in horizontal Mini/Micro channels. Cao et al. [10] investigated laminar convective heat transfer of supercritical CO_2 in horizontal miniature tube under cooling condition numerically. They believe that the results can benefit in the design and optimization of the PCHE with supercritical CO_2.

According to the authors knowledge, no DNS about the supercritical fluid flow in a horizontal pipe has been published, which can offer us an insight look of accurate flow mechanism without turbulence modelling. Through the current study, it is expected that the flow pattern of heated supercritical fluid in a horizontal pipe can be displayed and analysed by DNS. Various simulation

conditions will be reported. The pipe geometry is adjusted to D=1,2 mm, which is in the range of common PCHE channels. The influence of buoyancy to the heat transfer and flow turbulence of supercritical fluid is going to be our major consideration.

2. Computational details

2.1 Governing equations

In the present DNS study, supercritical CO_2 in the pipe is intensively heated by the constant and uniform wall heat flux q_w, which leads to significantly variable properties. Considering this, Navier-Stokes equations are constructed in low-Mach form Eqns.(1)-(3), in which the compressibility effect is excluded. This form of governing equations are also applied by other authors [5,6] in this area.

$$\frac{\partial(\rho)}{\partial t} + \frac{\partial(\rho U_j)}{\partial x_j} = 0 \qquad \text{Eqn. 1}$$

$$\frac{\partial(\rho U_i)}{\partial t} + \frac{\partial(\rho U_i U_j)}{\partial x_j} = -\frac{\partial P}{\partial x_i} + \frac{\partial}{\partial x_j}(\mu(\frac{\partial U_i}{\partial x_j} + \frac{\partial U_j}{\partial x_i})) \pm \rho g \delta_{i1} \qquad \text{Eqn. 2}$$

$$\frac{\partial(\rho h)}{\partial t} + \frac{\partial(\rho U_j h)}{\partial x_j} = \frac{\partial}{\partial x_j}(k\frac{\partial T}{\partial x_j}), \alpha = \frac{k}{\rho C_p} \qquad \text{Eqn. 3}$$

$$h = h(P_0, T), T = T(P_0, h), \rho = \rho(P_0, h), \mu = \mu(P_0, h), k = k(P_0, h), C_p = C_p(P_0, h) \qquad \text{Eqn. 4}$$

The governing equations Eqns. (1)-(3) are discretised with the open source finite-volume code OpenFOAM V2.4. The Pressure-Implicit with Splitting of Operators (PISO) algorithm is applied for pressure-velocity coupling. The temporal term is discretized with the second-order implicit Euler scheme. The spatial discretization is handled with central differencing scheme and a third-order upwind scheme QUICK is adopted for the convective term in the energy equation.
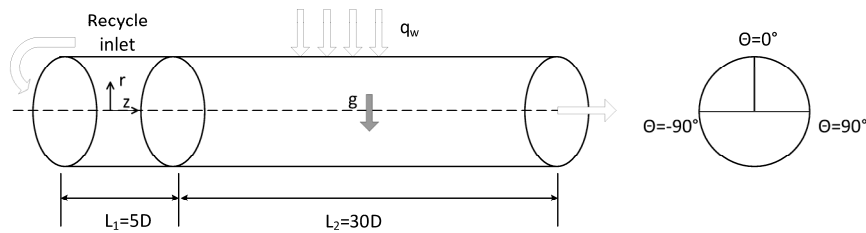

Figure 2: Geometry and boundary conditions

Fig.2 shows the pipe geometry and boundary conditions. At the inlet, an inflow generator of the length L_1=5D with an isothermal wall is adopted to generate approximately fully developed inflow turbulence. A recycling/rescaling procedure [11] is applied in this domain, which does not require any prior knowledge of turbulent flow profiles. For accelerating the turbulence development, the velocity field is initialized with perturbation method introduced by Schoppa and Hussain [12]. In

the second section of pipe L_2=30D, constant wall heat flux q_w is applied in the whole domain. The boundary condition of velocity field at outlet is the convective boundary condition $\frac{\partial(\emptyset)}{\partial t} + U_c \frac{\partial(\emptyset)}{\partial x} = 0$, where $\emptyset$ can be any any dependent variable, e.g. velocity U.

The cylindrical pipe is constructed with structured hexahedral mesh. The resolution is equivalent to approximately $168 \times 172 \times 400$ (radial r, circumferential θ and axial z direction) for the inflow domain and $168 \times 172 \times 2400$ for the heated domain, when converted from Cartesian to Cylindrical coordinates. The grid mesh is uniform spaced in the axial direction, and refined near the wall in the radial direction with a stretching ratio of 10, which corresponds to a dimensionless resolution of 0.11< Δy^+<1.1, $(R\Delta\theta)^+$≈6.5, Δz^+=4.6 in wall units, i.e.,$y^+ = yU_{\tau,o}/\nu$, based on inlet Reynolds number Re₀=5400. In the post processing, the mesh coordinate transform from Cartesian coordinate to Cylindrical coordinate is necessary. The flow statistics are obtained through averaging in time.

2.2 Simulation conditions

Simulation conditions of the present DNS are listed in Table 1. Inlet Re₀ is fixed to 5400 for the proper resolution. Pipe diameter are D=1,2 mm for the consideration of different buoyancy effect. Different wall heat flux q_w is also chosen as a variable.

Table 1: Simulation cases, Re₀=5400

Case	Type	P (MPa)	D (mm)	q_w (kW/m²)	q^+ *10⁴
SC160	Mixed	8	1	61.74	1.44
SC230F	Forced	8	2	30.87	1.44
SC230	Mixed	8	2	30.87	1.44
SC260	Mixed	8	2	61.74	1.44

2.3 Inflow turbulence

The quality of the inflow turbulence is validated with a better resolved reference DNS data by Wu and Moin [13] in 2008. This DNS is obtained using a second-order finite difference method. Grid points of $256 \times 512 \times 512$ are spaced in the L=7.5D long pipe at Re=5300. And the root-mean-square velocity in dimensionless form $U^+ = U/U_\tau$ of three directions is shown in Fig.3. The best agreement is observed in axial direction, because current dimensionless resolution is similar.
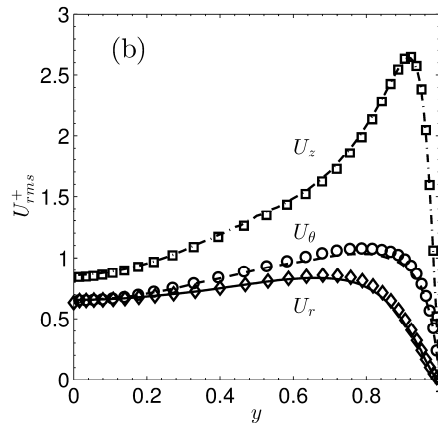
Figure 3: Inflow turbulence validation, dimensionless velocity fluctuation U_{rms}^+, lines: current DNS at Re$_0$=5400, symbols: DNS data from Wu and Moin [13] at Re=5300

3. Results and discussion

3.1 Bulk properties

Fig.4a summarizes the development of wall temperature T_w on top- and bottom surface of the pipe. T_w is homogeneously distributed in circumferential direction in force-convection case SC230F. Buoyancy leads to a non-uniform distribution of wall temperature in circumferential direction. In SC160, SC230 and SC260, T_w is significantly higher on the top surface than bottom surface. On the top surface, T_w shows a monotically rising tendency in three cases, where the highest T_w distribution is found in SC260 due to high T_w. At the end of the pipe z=30D, temperature difference ΔT_w between top- and bottom surface is 365.2K (SC260), 234.2K (SC230) and 136.1K (SC160).

Streamwise distribution of local Nusselt number Nu$=\dfrac{h(D)}{\kappa}$ of top- and bottom surfaces is given in Fig.4b, where h is convective heat transfer coefficient and κ is thermal conductivity evaluated with local bulk temperature T_b. Here, Nusselt number (Nu) on bottom surface is greatly higher than on top surface in all buoyancy relevant cases. It indicates a great difference of convective heat transfer on both sides of wall surfaces. In SC230 and SC260, the distribution of Nu on the top surface is close with each other after about z=10D, although SC260 is applied with double wall heat flux as SC230. But as for the bottom surface, Nu from SC230 is significantly higher than from SC260, which means that the biggest ΔNu is found in SC230. The smallest ΔNu is found in SC160, which means buoyancy has less influence on heat transfer for pipe with smaller radius (D=1 mm against D=2 mm).
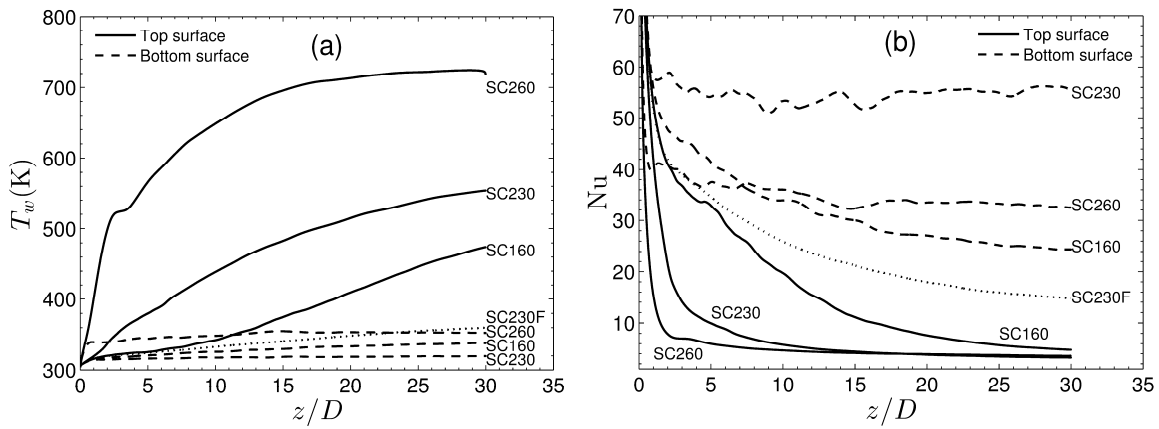
Figure 4: Development of T_w (a) and Nu (b) in downstream direction

The skin friction coefficient distribution $C_f = 2\tau_w/(\rho_b U_b^2)$ based on local wall shear stress is summarized in Fig.5. At the inlet, C_f=0.00896 matches Blasius estimation $C_f = 0.079\text{Re}^{-0.25}$=0.00897 with 0.15% difference. In the downstream direction, C_f on bottom of pipe is higher than top surface in SC160 and SC230. On bottom surface, C_f in SC230 and SC260 shows similar development. But on the top surface, SC260 shows an obvious increasing tendency after about z=3D, which is not clearly observed in SC230. Fig.6 shows the distribution of C_f in circumferential direction θ. Unlike T_w in Fig.5, a monotical tendency in the half circumference is not observed in C_f. At z=25D of SC160, C_f shows a near flat distribution at about -20°< θ <20° near the top surface. Observing from bottom- to the top surface (θ =±180°) in SC230 and SC260, C_f begins to decrease to the minimum firstly and rises up again.
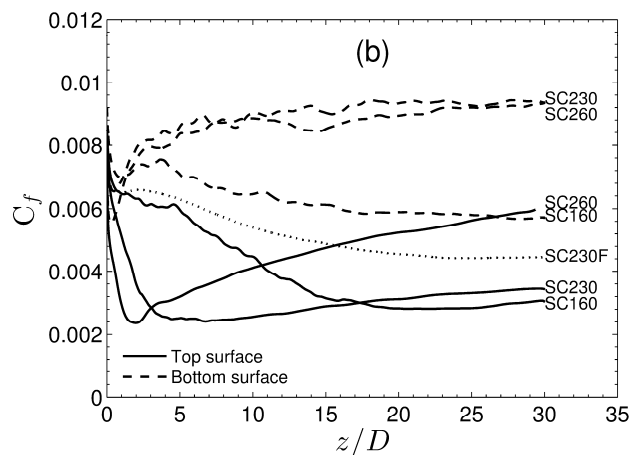

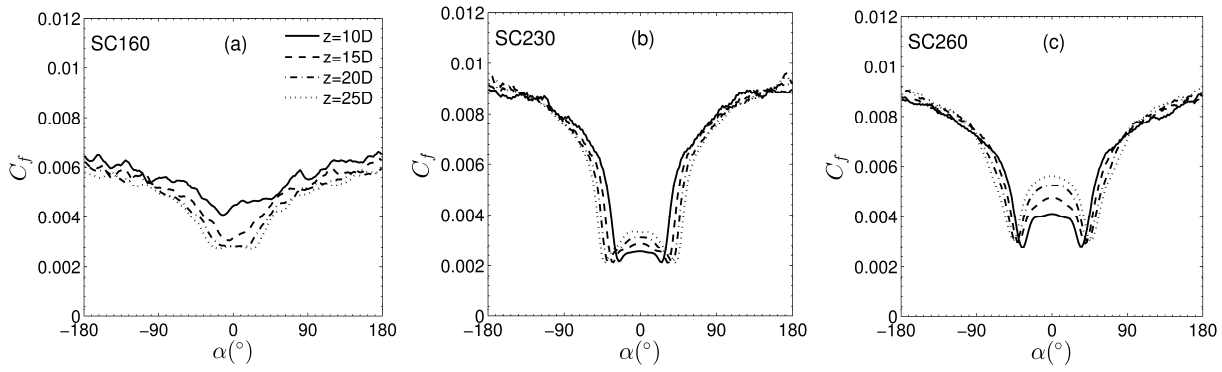Figure 5: Evaluation of C_f in downstream direction

6

Figure 6: Distribution of C_f in circumferential direction, (a): SC160, (b): SC230 and (c): SC260

Richardson number Ri is often applied for quantification of stratified flow due to buoyancy. The evaluation of Richardson number Ri=Gr/Re^2 is given in Fig.7. It indicates the relation between natural convection to forced convection. Cases with Ri>0.1 is expected to be buoyancy relevant. SC230 and SC260 exceed this value on both surfaces in downstream direction, and SC160 shows about one order lower Gr/Re^2 as a result of smaller pipe diameter.
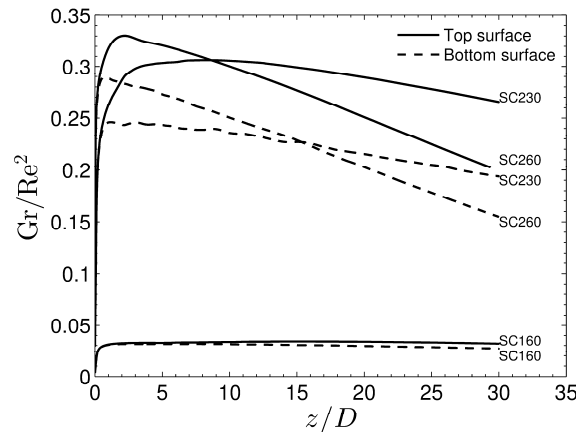
Figure 7: Evaluation of Gr/Re^2 in downstream direction on top- and bottom surfaces

3.2 Flow statistics

Compared with SC160, stronger buoyancy effect in SC230 leads to a deformation of average velocity profile as in the first row of Fig.8. At *z=10D*, high-velocity fluid with low density begins to concentrate in the bottom section and low-velocity fluid with low density occupies the upper part of pipe cross section. High-velocity fluid becomes to a crescent shape at this position. At *z=15D* and *20D*, a small area of high velocity fluid is developed close to the top wall surface and it connects with the major part of high-velocity fluid at *z=25D*. The high-speed fluid is found to be an anchor shape at this position. The quantitative analyse of velocity field at *z=25D* is as shown in Fig.9. At θ =0°, a velocity peak is observed at about r/R=0.75, which corresponds to the high-speed region near the top wall. Compared with that, velocity profile at θ =45° shows a low value from *r/R*=0.4 to *r/R*=0.9, which is also visualized in Fig.8. This can be explained by the transport of secondary flow. Low-velocity flow close to the circumferential wall flows upwards due to low density and drops down at about θ =45°. Therefore, a low velocity region is developed here.

7

The stratification of temperature field is similar as in SC160. The hot fluid gathers near the top surface and it shows a significant temperature difference against the cold fluid on the bottom. Compared with SC160, this hot layer becomes thicker. This change of temperature field is also reflected in the density field in the third row. Due to buoyancy, hot CO_2 with low density concentrates on the upper side of cross section. With the input of wall heat flux, low density layer is growing in downstream direction.
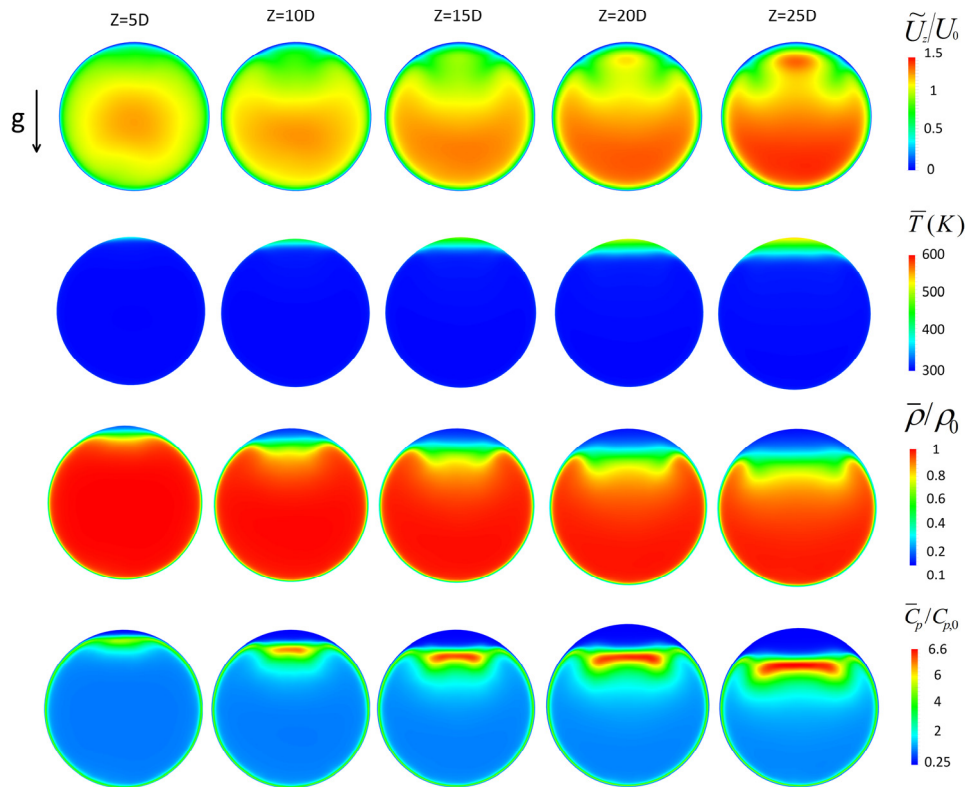
Figure 8: Flow field of SC230 in downstream direction, velocity, temperature, density, special thermal capacity

Vector plot of 2-D average velocity field on the cross section are given in Fig.10. The lines are coloured with normalized density value. The visualization shows that buoyancy brought by enormous density difference leads to the formation of secondary flow. Following the path of velocity in all four figures in SC230, it is observed that fluid near the circumferential wall (marked in blue) is heated by wall heat flux q_w firstly, which leads to a significant decrease of fluid density. As a result of buoyancy, this low-density flow near wall flows upward along the wall surface and meet at near the top surface. And then it falls down in the gravitational direction along the centreline. The two vortex centre of secondary flow locates near axis-symmetrically on the lateral sides. At these four streamwise positions, the positions of vortex centre are slightly different. Comparing the figures horizontally (*z=10D to z=15D, z=20D to z=25D*), vortex centre seems to move downwards. In downstream direction, the stratified layer with low-density fluid is growing progressively. But the centres of vortex from the secondary flow is always filled with high-density

fluid (coloured in red) but locate just slightly below the buffer layer between high- and low-density, which is coloured in yellow in the figure.
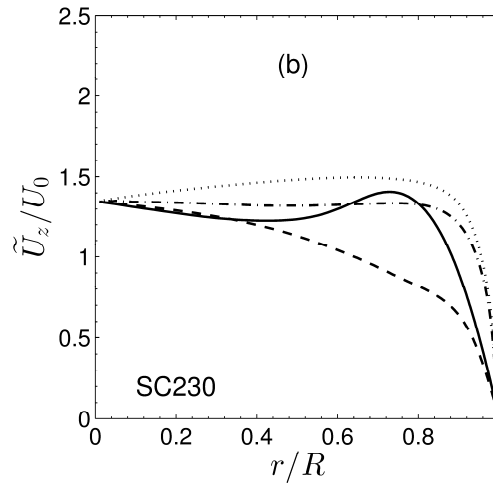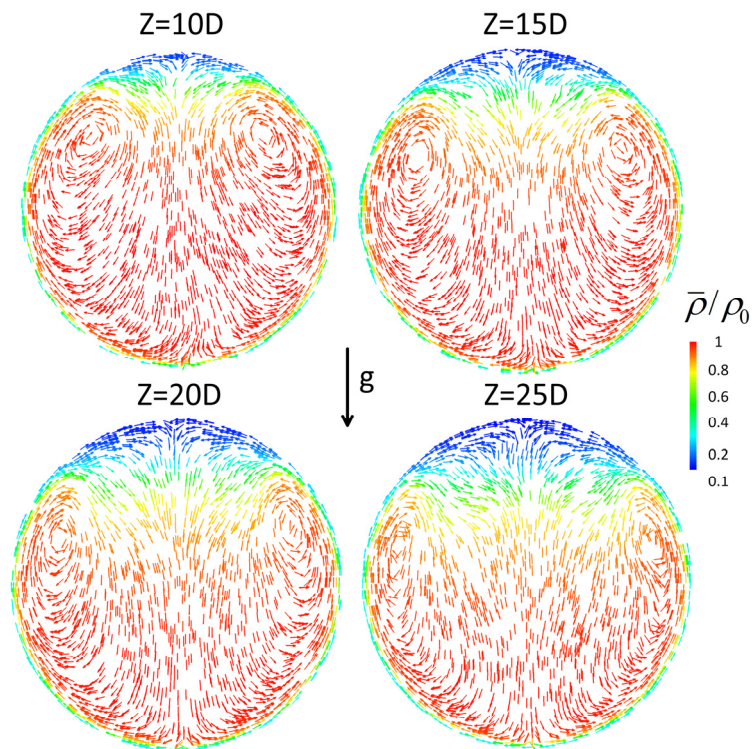

Figure 9: velocity profile of SC230 at *z=25D*

Figure 10: vector plot of 2-D velocity profile of SC230 at *z=25D*

Fig.11 shows the velocity vector plot of SC230 at *z=25D*, coloured by TKE and its components in three directions ($\overline{U_{rr}^{''}{}^{2}}$, $\overline{U_{\theta\theta}^{''}{}^{2}}$ and $\overline{U_{zz}^{''}{}^{2}}$) respectively. The thin layer of fluid closest the circumferential wall (colored with dark blue) locates in the laminar sublayer and has the lowest TKE. It is transported to the top surface by sescondary flow in circumferential direction. It is collected near the top wall surface and builds up an area which shows lowest velocity fluctuation in all three directions. Flow around the vortex centres of secondary flow shows relatively high TKE.

Highest TKE is found between the wall and vortex centres laterally. Peak value of $\overline{U_{rr}^{"}}^{2}$ is observed on the flow near the vortex center at the side of axis of symmetry, where the secondary flow is bended to pipe center. Peak value of $\overline{U_{\theta\theta}^{"}}^{2}$ locates also near the vortex centers but on the side of the wall. As the dominant component of TKE, the distribution of $\overline{U_{zz}^{"}}^{2}$ is largely similar as that of TKE.
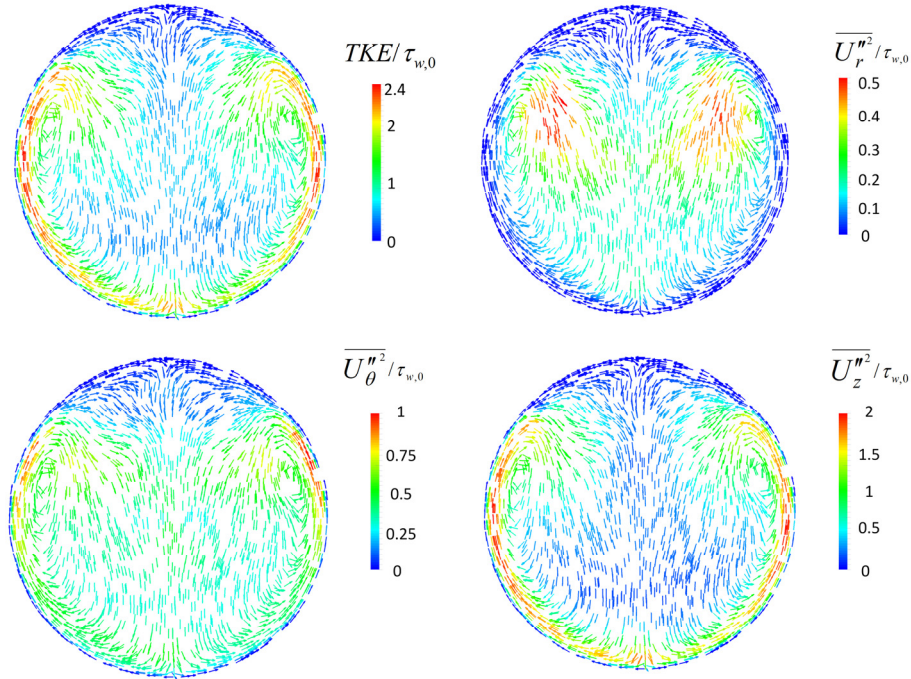

Figure 11: vector plot of 2-D velocity profile with velocity fluctuations of SC230 at *z=25D*

Production rate of turbulent kinetic energy (*Pk*) at different circumferential position on *z=25D* is shown in Fig.12a, where *Pk* is defined as $Pk = \overline{\rho U_i U_j} \frac{\widetilde{U}_i}{x_j}$. The isothermal flow at *z=0D* is marked with symbol as a reference. In SC230, *Pk* almost vanishes at *θ=0°*, which explains the significantly reduced TKE at this position in Fig. 12b. The profile at *θ=45°* shows a sign change near *r/R=0.8*, which is relevant with the secondary flow at this position. *Pk* at *θ=90°* is with a reduced peak value, where *Pk* at *θ=180°* shows a higher peak. For the pipe bulk area *0<r/R<0.9*, *Pk* is significantly reduced at *θ=0°, 90°, 180°*. In SC260, *Pk* shows a slight double peak character at *ϑ=0°*. The first peak near the wall can be explained with the increased velocity gradient brought by flow acceleration as shown in Fig.7. At *θ=45°*, *Pk* shifts its peak to *r/R=0.7* under the influence of secondary flow. At *θ=90°* and *θ=180°*, narrow peak with a maximum close to the original value is observed in the figure.
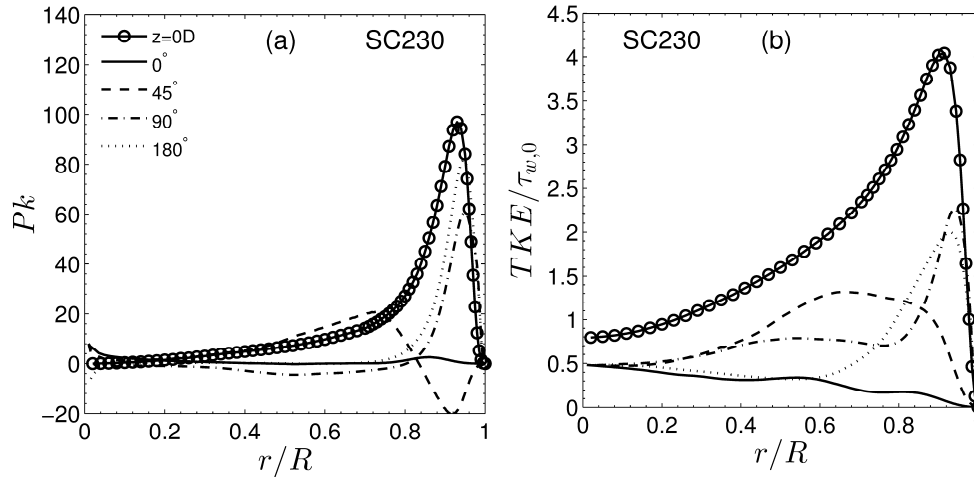
Figure 12: *Pk* and TKE of SC230 at z=25D

4. Conclusions

In the current research, heat transfer of supercritical CO_2 in a horizontal pipe has been investigated using direct numerical simulation (DNS) for the first time. Well resolved DNS eliminates the uncertainty brought by turbulence modelling and gives us the opportunity to discover the stratification in turbulent fluid field directly. The small pipe diameter ($D=1, 2$ mm) and moderately low inlet Reynolds number $Re_0=5400$ is similar as the channel flow in the compact heat exchanger (PCHE). Inlet flow temperature (T_0) is slightly lower than pseudo-critical temperature T_{pc}. A rapid change of thermos-physical properties occurs, when fluid temperature rises across T_{pc} under heating condition. Following interesting points are concluded from the current research:
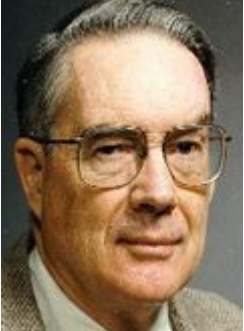
1. Wall temperature T_w is found to be strongly inhomogeneous in the circumferential direction. T_w is gratefully higher on the top surface than on the bottom surface. Stronger buoyancy effect is found in the pipe with larger diameter (SC230 and SC260). Buoyancy also leads to an inhomogeneously distributed skin friction coefficient C_f in the circumferential direction.

2. As a result of buoyancy, flow stratification occurs in the pipe flow. Secondary flow is built up due to density difference and it transports the heated fluid to the top surface. Therefore, high-temperature fluid with extremely low density is collected in this region, which explained the high wall temperature on the top wall surface.

3. The streamwise velocity field $\widetilde{U}_z$ is also modified by the flow stratification. Low-speed fluid close to the circumferential wall is heated firstly and transported to the top by the secondary flow. High-speed bulk fluid settles at the bottom as a result of high density. In SC230 and SC260, anchor shape high-speed velocity profile is observed as a result of the motion of low-speed velocity $\widetilde{U}_z$ near the wall.

4. This modification of average velocity field has also shown influence to the flow turbulence in case SC230. Reduced velocity gradient near the top wall prevents the turbulence production from shear. As a result, turbulent kinetic energy is strongly suppressed which is also the same in the

field of radial turbulent heat flux in this direction $\theta=0°$. It indicates an attenuated convective heat transfer in this direction and enhances the flow stratification.

5. References

[1] V. Dostal, M. J. Driscoll, P. Hejzlar, A supercritical carbon dioxide cycle for next generation nuclear reactors, Ph.D. thesis (2004).

[2] R. B. Duffey, I. L. Pioro, Experimental heat transfer of supercritical carbon dioxide flowing inside channels (survey), Nuclear Engineering and Design 235 (8) (2005) 913-924.

[3] J. D. Jackson, Fluid ow and convective heat transfer to fluids at supercritical pressure, Nuclear Engineering and Design 264 (2013) 24-40.

[4] S. He, W. S. Kim, J. H. Bae, Assessment of performance of turbulence models in predicting supercritical pressure heat transfer in a vertical tube, International Journal of Heat and Mass Transfer 51 (19-20) (2008)

[5] J. H. Bae, J. Y. Yoo, H. Choi, Direct numerical simulation of turbulent supercritical flows with heat transfer, Physics of Fluids 17 (10) (2005)

[6] H. Nemati, A. Patel, B. J. Boersma, R. Pecnik, Mean statisticsof a heated turbulent pipe ow at supercritical pressure, International Journal of Heat and Mass Transfer 83 (2015) 741-752.

[7] G. A. Adebiyi, W. B. Hall, Experimental investigation of heat transfer to supercritical pressure carbon dioxide in a horizontal pipe, International Journal of Heat and Mass Transfer 19 (7) (1976) 715-720.

[8] M. Bazargan, D. Fraser, Heat transfer to supercritical water in a horizontal pipe: modeling, new empirical correlation, and comparison against experimental data, Journal of Heat Transfer 131 (6) (2009) 061702.

[9] S. Liao, T. Zhao, Measurements of heat transfer coefficients from supercritical carbon dioxide flowing in horizontal mini/micro channels, Journal of Heat Transfer 124 (3) (2002) 413-420.

[10]   X. Cao, Z. Rao, S. Liao, Laminar convective heat transfer of supercritical CO$_2$ in horizontal miniature circular and triangular tubes, Applied Thermal Engineering 31 (14) (2011) 2374-2384.

[11]   T. S. Lund, X. Wu, K. D. Squires, Generation of turbulent inflow data for spatially-developing boundary layer simulations, J. Comput. Phys.140 (2) (1998) 233-258.

[12]   W. Schoppa, F. Hussain, Coherent structure dynamics in near wall turbulence, Fluid Dynamics Research 26 (2) (2000) 119-139.

[13]   X. Wu, P. Moin, A direct numerical simulation study on the mean velocity characteristics in turbulent pipe flow, Journal of Fluid Mechanics 608 (2008) 81-112.

Table 2: Author information

	Xu Chu Ph.D. candidate at IKE, University of Stuttgart, Germany
	Eckart Laurien, Prof. Dr. –Ing, Professor at IKE, University of Stuttgart, Germany
	Donald McEligot, Prof. Professor Emeritus Distinguished Visiting Professor, University of Idaho, USA